

# Ray-tracing and physical-optics analysis of the aperture efficiency in a radio telescope

Luca Olmi<sup>1,2</sup> and Pietro Bolli<sup>3,4</sup>

<sup>1</sup>*INAF, Istituto di Radioastronomia, sezione di Firenze, Largo E. Fermi 5, I-50125*

*Firenze, Italy*

<sup>2</sup>*University of Puerto Rico, Rio Piedras Campus, Physics Dept., Box 23343, UPR*

*Station, San Juan, PR 00931-3343, USA*

<sup>3</sup>*INAF, Osservatorio Astronomico di Cagliari, Loc. Poggio dei Pini, Strada 54,*

*I-09012, Cagliari, Italy*

<sup>4</sup>*INAF, Istituto di Radioastronomia, sezione di Bologna, Via P. Gobetti 101,*

*I-40129 Bologna, Italy*

*olmi@arcetri.astro.it*

The performance of telescope systems working at microwave or visible/IR wavelengths is typically described in terms of different parameters according to the wavelength range. Most commercial ray tracing packages have been specifically designed for use with visible/IR systems and thus, though very flexible and sophisticated, do not provide the appropriate parameters to fully describe microwave antennas, and thus to compare with specifications. In this work we demonstrate that the Strehl ratio is equal to the phase efficiency when the apodization factor is taken into account. The phase efficiency is the most critical contribution to the aperture efficiency of an antenna, and the most difficult parameter to optimize during the telescope design. The equivalence between the Strehl ratio and the phase efficiency gives the designer/user of the telescope the opportunity to use the faster commercial ray-tracing software to optimize the design. We also discuss the results of several tests performed to check the validity of this relationship that we carried out using a ray-tracing software, ZEMAX and a full Physical Optics software, GRASP9.3, applied to three different telescope designs that span a factor of  $\simeq 10$  in terms of  $D/\lambda$ . The maximum measured discrepancy between phase efficiency and Strehl ratio varies between  $\simeq 0.4\%$  and  $1.9\%$  up to an offset angle of  $> 40$  beams, depending on the optical configuration, but it is always less than  $0.5\%$  where the Strehl ratio is  $> 0.95$ .

*OCIS codes:* 000.0000, 999.9999.

## 1. Introduction

Performance evaluation is a critical step in the design of any optical system, either at microwave or visible/IR wavelengths. The image quality criteria more commonly used, however, are quite different in these two regions of the electromagnetic spectrum. In fact, in the analysis of microwave antennas and radio telescopes the two fundamentals figures-of-merit used by designers and users are the aperture efficiency and the beam efficiency, whereas in optical systems the Strehl ratio and ray aberrations are often quoted. This is because of the *coherent* nature of most microwave antennas, where single-moded receivers are generally used (exceptions may be millimeter and submillimeter bolometers used in radio astronomy), making the phase distribution in the image as important as the amplitude distribution in determining the performance of the optics. In fact, the aperture efficiency is intrinsically dependent on the phase distributions since it is calculated as a correlation integral between the focal region field produced by an incident plane wave and the horn aperture field.

The difference between the microwave and visible/IR wavelengths regimes, in terms of the image quality criteria applied to astronomical telescopes, has been reduced over the past 10-15 years thanks to the development of focal plane arrays (FPA, hereafter). In fact, the noise performance of receivers used in radio astronomy has improved dramatically during this time, especially at millimeter and submillimeter

wavelengths. As a consequence, it has become clear that the best means of increasing observing efficiency for mapping extended sources or to conduct blind searches is to use imaging arrays located at the focal plane of the telescope. This implies the need of a larger field of view (FOV) with few aberrations in the range of frequencies used by the array(s) of receivers. Very often these FPA require some relay optics to convert the telescope focal ratio (which, in some cases, may be quite large, i.e.  $\gtrsim 10$ ) to the smaller focal ratios of the individual feed-horns. As a consequence, the overall image quality of the *total* system, telescope and reimaging optics, must be evaluated over a wide FOV, thus effectively contributing to bridging the gap between the microwave and visible wavelengths regimes.

A number of commercial ray tracing packages exist that are being used to analyse the performance of FPAs for use with existing or planned (sub)millimeter telescopes. However, many of these packages have been specifically designed for use with optical (i.e., visible and IR) systems and thus, although very flexible and sophisticated, they do not provide the appropriate parameters to fully describe microwave antennas, and thus to compare with specifications. The possibility to easily convert an optical-based design parameter, such as the Strehl ratio, to a fundamental antenna-based design parameter, such as the phase efficiency, gives the designer/user of the telescope the opportunity to use the faster commercial ray-tracing software to optimize the design. Once the design is optimized, a full Physical Optics software can be used to analyse more thoroughly all critical performance parameters of the antenna (e.g., spillover,

antenna noise temperature, etc.). Another advantage offered by this conversion consists of the possibility to study the degrading effects on the wavefront caused by obstructions to the beam (e.g., secondary reflector and its support struts) which are notoriously difficult to simulate in Physical Optics software.

In this paper we review the main design parameters generally used in evaluating the performance of optical designs at both microwave and visible wavelengths. Based on this review we find a simple relationship between the (antenna-based) aperture efficiency and the Strehl ratio. We also show the results of several tests performed to check the validity of this relationship that we carried out using a ray-tracing software, ZEMAX and a full Physical Optics software, GRASP9.3, applied to three different telescope designs.

The paper is organized as follows: In Sect. 2 we review and discuss the definitions of antenna gain and aperture efficiency while in Sect. 3 we analyse the definition of Strehl ratio and derive a simple relationship between the aperture efficiency and the Strehl ratio; in Sect. 4 we show the results of a comparison obtained using a Physical Optics and a ray-tracing program and, finally, we draw our conclusions in Sect. 5.

## 2. Antenna gain and aperture efficiency

### 2.A. Definitions

The gain of an antenna is a measure of the coupling of the antenna to a plane wave field, and it can be written in terms of the *effective area* (we assume that ohmic losses

are negligible):

$$G(\theta, \phi) = \frac{4\pi}{\lambda^2} A_{eff}(\theta, \phi). \quad (1)$$

For an aperture type antenna the gain is expressible in terms of the illumination by the feed. We can assume that the illumination is linearly polarized, and that the aperture lies on an infinite plane. In this case the gain is expressible in terms of  $E_a(\mathbf{r}')$ , the magnitude of the (in-phase) illuminating electric field in the aperture plane. If almost all of the energy in the field is contained in a small angular region about the  $z'$  axis, and if we use the scalar-field approximation, then  $G(\theta, \phi)$  can be written as:<sup>1</sup>

$$G(\theta, \phi) = \frac{4\pi}{\lambda^2} \frac{\left| \int_{AP'} \mathcal{E}_a(\mathbf{r}', \hat{\mathbf{R}}) dS' \right|^2}{\int_{\infty} E_a^2(\mathbf{r}') dS'}, \quad (2)$$

with

$$\mathcal{E}_a(\mathbf{r}', \hat{\mathbf{R}}) \equiv E_a(\mathbf{r}') e^{j\Phi(\mathbf{r}')} e^{jk\hat{\mathbf{R}} \cdot \mathbf{r}'} \quad (3)$$

$$\hat{\mathbf{R}} \cdot \mathbf{r}' = r' \sin \theta \cos(\phi - \phi')$$

$$dS' = r' dr' d\phi'$$

where we have introduced the complex electric field in the aperture,  $\mathcal{E}_a(\mathbf{r}', \hat{\mathbf{R}})$ . We have also indicated with  $k = 2\pi/\lambda$  the wavenumber, and the field point Q at position  $\mathbf{r}'$  on the aperture plane (see Fig. 1) has polar coordinates  $(r', \phi')$ .  $\hat{\mathbf{R}}$  is the unit vector along the direction to the observation point, with  $\theta$  representing the angle formed by the direction to the observation point and the optical axis and  $\phi$  being the angle measured in the plane of scan, i.e. perpendicular to the optical axis ( $\hat{\mathbf{z}}'$ ), as shown

in Fig. 1. The integral in the numerator is calculated over the antenna aperture, whereas the integral in the denominator must extend over the entire plane if there is any spillover illumination in the case of reflector antennas.

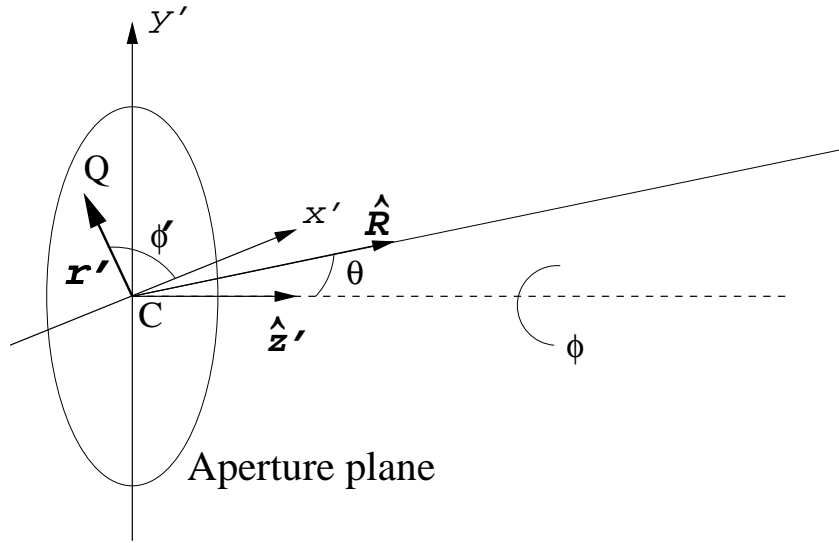


Fig. 1. Coordinate systems used to calculate the antenna gain.

The phase aberration function,  $\Phi(\mathbf{r}')$ , in Eq. (3) defines the phase at point  $\mathbf{r}'$  in the aperture plane, which accounts for any change in the optical path length resulting from the structural deformation of the primary reflector, the displacements of the secondary reflector and the feed. Thus, it is in  $\Phi(\mathbf{r}')$  that one can take into account the positions of different feed-horns in a FPA.

For aperture type antennas, the effective aperture can be related directly to the antenna geometric area,  $A_g$ , by means of the *aperture efficiency*,  $\eta_A(\theta, \phi)$  (e.g., see Ref. 2),

$$A_{eff}(\theta, \phi) = A_g \eta_A(\theta, \phi). \quad (4)$$

Therefore,

$$G(\theta, \phi) = \frac{4\pi A_g}{\lambda^2} \eta_A(\theta, \phi) \quad (5)$$

$$\eta_A(\theta, \phi) = \frac{\left| \int_{AP'} \mathcal{E}_a(\mathbf{r}', \hat{\mathbf{R}}) dS' \right|^2}{A_g \int_{\infty} E_a^2(\mathbf{r}') dS'}. \quad (6)$$

The on-axis gain,  $G_o$ , is obtained by setting  $\hat{\mathbf{R}} \cdot \mathbf{r}' = 0$ , then we obtain:

$$G_o = \frac{4\pi A_g}{\lambda^2} \eta_o \quad (7)$$

$$\eta_o = \frac{\left| \int_{AP'} E_a(\mathbf{r}') e^{j\Phi(\mathbf{r}')} dS' \right|^2}{A_g \int_{\infty} E_a^2(\mathbf{r}') dS'}. \quad (8)$$

If the phase is constant over the aperture the on-axis gain attains its maximum value,

$G_M$ :

$$G_M = \frac{4\pi A_g}{\lambda^2} \eta_M \quad (9)$$

$$\eta_M = \frac{\left| \int_{AP'} E_a(\mathbf{r}') dS' \right|^2}{A_g \int_{\infty} E_a^2(\mathbf{r}') dS'}. \quad (10)$$

A case of special interest is that of uniform illumination over the aperture, i.e.,

$E_a(\mathbf{r}') = const$  over the antenna aperture and zero outside. Hence, we obtain  $\eta_M = 1$

and the *ideal gain*,  $G_{\text{ideal}}$ , is then defined as

$$G_{\text{ideal}} = \frac{4\pi A_g}{\lambda^2} \geq G_M. \quad (11)$$

Thus, we obtain the well-known result that the uniform field distribution over the aperture gives the highest gain of all constant-phase distributions over the aperture.<sup>1</sup>

### 2.B. Phase-error effects

In the previous section we showed that if the phase distribution is constant over the aperture, the maximum gain,  $G_M$ , is obtained in the direction of the optical axis, i.e.  $\hat{\mathbf{R}} \cdot \mathbf{r}' = 0$ . However, if a phase-error distribution is present over the aperture, this may no longer be the case. A phase-error over the aperture, i.e. deviations from uniform phase, may arise from various causes, such as a displacement of the feed-horn from the on-axis focus (e.g., in FPAs), or distortion of the optical surfaces, or it may be caused by phase-error in the field of the feed-horn.

If the phase distribution is a *linear* function of the aperture coordinates, then it can be shown that the far-field is the same as that of the constant-phase distribution but displaced with respect to the  $z'$ -axis, i.e. the direction of peak-gain is no longer in the direction of the system optical axis.<sup>1</sup> In the case of arbitrary phase distributions over the aperture, if the phase-error does not deviate too widely from constant phase over the aperture, and if it can be decomposed into a linear phase distribution and higher-order terms, then we may write

$$\Phi(\mathbf{r}') = \Phi_1(\mathbf{r}') + \Phi_{ab}(\mathbf{r}') \quad (12)$$

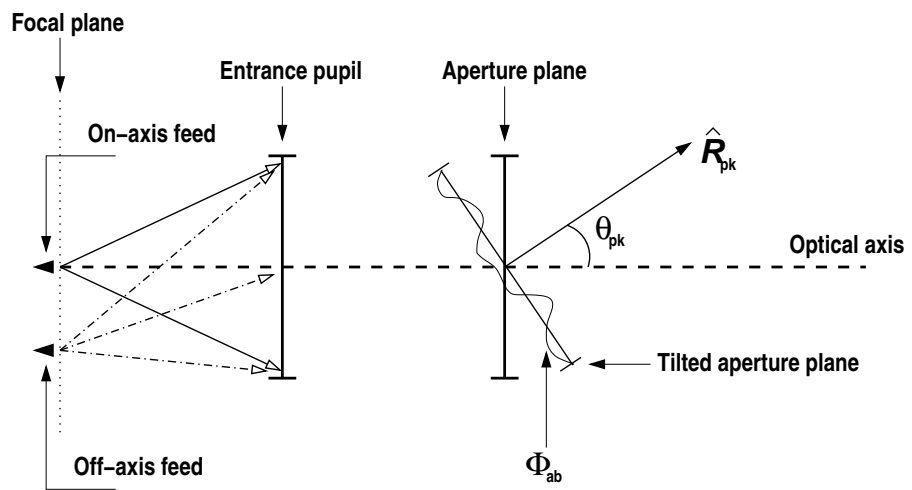


Fig. 2. Off-axis feed and tilted aperture plane geometry.

where  $\Phi_1(\mathbf{r}')$  is linear in the coordinates over the aperture and causes an undistorted beam shift, i.e. a change in direction of the peak gain (now corresponding to  $\theta = \theta_{\text{pk}}$ ), whereas  $\Phi_{ab}(\mathbf{r}')$  accounts for the true wave front distortion. The shifted far-field beam can then be considered to have arisen from a tilted aperture plane, i.e., from the aperture projected onto a plane normal to the direction of the peak gain,  $\hat{\mathbf{R}}_{\text{pk}}$ , as shown in Fig. 2. In the projected aperture the linear phase distribution term cancels out, leaving only higher-order phase errors, i.e.,

$$\eta_A(\theta, \phi) = \frac{\left| \int_{AP} \mathcal{E}_a(\mathbf{r}, \hat{\mathbf{R}}) dS \right|^2}{A_g \int_{\infty} E_a^2(\mathbf{r}) dS}, \quad (13)$$

where now

$$\mathcal{E}_a(\mathbf{r}, \hat{\mathbf{R}}) \equiv E_a(\mathbf{r}) e^{j\Phi_{ab}(\mathbf{r})} e^{jk\hat{\mathbf{R}} \cdot \mathbf{r}}, \quad (14)$$

and where  $\mathbf{r}$  is the position of a point in the projected aperture plane, indicated with  $AP$ , such that  $\hat{\mathbf{R}} \cdot \mathbf{r} = 0$  for  $\hat{\mathbf{R}} = \hat{\mathbf{R}}_{\text{pk}}$ . If  $\Phi_{ab}(\mathbf{r}) = 0$  then the field distribution has constant phase over the projected aperture and the antenna gain in this aperture will be given by,<sup>1</sup>

$$G_{\text{MP}} = G_{\text{M}} \cos \theta_{\text{pk}} \quad (15)$$

where  $\cos \theta_{\text{pk}} \simeq 1$  for most radio astronomical applications. Therefore, in the following sections we will refer to the antenna gain and aperture efficiency as the gain and aperture efficiency in the projected aperture plane, unless noted otherwise.

### 2.C. Main contributions to the aperture efficiency

The aperture efficiency of an antenna is determined by a number of phenomena and hence it can be written as the product of a number of individual contributions (e.g., see Ref. 3):

$$\eta_A(\theta, \phi) = \eta_{\text{spill}} \eta_{\text{taper}}(\theta, \phi) \eta_{\text{phase}}(\theta, \phi) \quad (16)$$

where  $\eta_{\text{spill}}$  is the *spillover efficiency*,  $\eta_{\text{taper}}$  is the *taper efficiency* and  $\eta_{\text{phase}}$  takes into account all *phase-error effects* causing a distortion of the wave front. We have also assumed that ohmic losses are negligible and that the aperture is unblocked. The spillover efficiency includes all spillover contributions from the feed, subreflector, diffraction, etc.,

$$\eta_{\text{spill}} = \frac{\int_{AP} E_a^2(\mathbf{r}) dS}{\int_{\infty} E_a^2(\mathbf{r}) dS}. \quad (17)$$

$\eta_{\text{taper}}$  accounts for the aperture illumination taper due to the feed and the reflector geometry,

$$\eta_{\text{taper}}(\theta, \phi) = \frac{\left| \int_{AP} E_a(\mathbf{r}) e^{j k \hat{\mathbf{R}} \cdot \mathbf{r}} dS \right|^2}{A_g \int_{AP} E_a^2(\mathbf{r}) dS}, \quad (18)$$

and finally,  $\eta_{\text{phase}}$  accounts for the residual high-order phase distortions of the wave-front at the aperture plane, due to optical aberrations, surface errors or misalignments,

etc.,

$$\eta_{\text{phase}}(\theta, \phi) = \frac{\left| \int_{AP} \mathcal{E}_a(\mathbf{r}, \hat{\mathbf{R}}) dS \right|^2}{\left| \int_{AP} E_a(\mathbf{r}) e^{jk\hat{\mathbf{R}} \cdot \mathbf{r}} dS \right|^2}. \quad (19)$$

In the direction of the peak gain  $\hat{\mathbf{R}} \cdot \mathbf{r} = 0$ , as we earlier mentioned, and thus the  $\hat{\mathbf{R}} = (\theta, \phi)$  dependence can be dropped from  $\eta_{\text{taper}}$  and  $\eta_{\text{phase}}$ .

In the case of on-axis, dual-reflector systems the central subreflector and its support structure cause a partial shadowing of the aperture, which leads to a loss of efficiency. To take this effect into account the integral at the numerator of Eq. (13) can be written in the case of a partially blocked aperture:

$$\int_{AP_{\text{block}}} \mathcal{E}_a(\mathbf{r}, \hat{\mathbf{R}}) dS = \int_{AP} \mathcal{E}_a(\mathbf{r}, \hat{\mathbf{R}}) dS - \int_{subr} \mathcal{E}_a(\mathbf{r}, \hat{\mathbf{R}}) dS \quad (20)$$

where  $AP_{\text{block}}$  represents the area of the aperture plane subtracted of the blocked part,  $AP$  indicates as usual the full area of the aperture plane and  $subr$  indicates the integration area over the subreflector, assuming this is the main source of blockage.

By substituting Eq. (20) into Eq. (13) we thus obtain,

$$\begin{aligned} \eta_A(\theta, \phi) &= \frac{\left| \int_{AP} \mathcal{E}_a(\mathbf{r}, \hat{\mathbf{R}}) dS \right|^2}{A_g \int_{\infty} E_a^2(\mathbf{r}) dS} \times \\ &\quad \left| 1 - \frac{\int_{AP} \mathcal{E}_a(\mathbf{r}, \hat{\mathbf{R}}) dS}{\int_{AP} \mathcal{E}_a(\mathbf{r}, \hat{\mathbf{R}}) dS} \right|^2 \end{aligned} \quad (21)$$

where the first term at the right can once again be written as in Eq. (16) and thus

the second term can be interpreted as the *blocking efficiency* due to the subreflector,

$$\eta_{\text{block}}(\theta, \phi) = \left| 1 - \frac{\int_{AP} \mathcal{E}_a(\mathbf{r}, \hat{\mathbf{R}}) dS}{\int_{A_{\text{subr}}} \mathcal{E}_a(\mathbf{r}, \hat{\mathbf{R}}) dS} \right|^2. \quad (22)$$

We note that in the direction of the peak-gain ( $\hat{\mathbf{R}}_{\text{pk}} \cdot \mathbf{r} = 0$ ), for an uniform, unaberrated ( $\Phi_{ab}(\mathbf{r}) = 0$ ) field we find the well-known result,

$$\eta_{\text{block}} = \left( 1 - \frac{A_{\text{subr}}}{A_{\text{prim}}} \right)^2 \quad (23)$$

where  $A_{\text{prim}}$  and  $A_{\text{subr}}$  are the surface areas of the primary and secondary reflectors, respectively. In general, the geometrical blockage caused by the support struts can be up to several times larger than the blockage caused by the secondary mirror, especially in open-air antennas. Therefore, the blockage efficiency given by Eq. (23) usually overestimates the real efficiency and should be corrected including the strip blockage of the plane-wave and the blockage from the converging spherical-wave between the primary mirror and the subreflector (e.g., see Ref. 4).

### 3. Strehl ratio

#### 3.A. Strehl ratio on-axis

While the main antenna-based figures-of-merit are usually, though not necessarily, defined in the far field of the aperture, the Strehl ratio of an optical imaging system is defined as the ratio of the aberrated to unaberrated incoherent Point Spread Function (PSF, hereafter<sup>5</sup>).

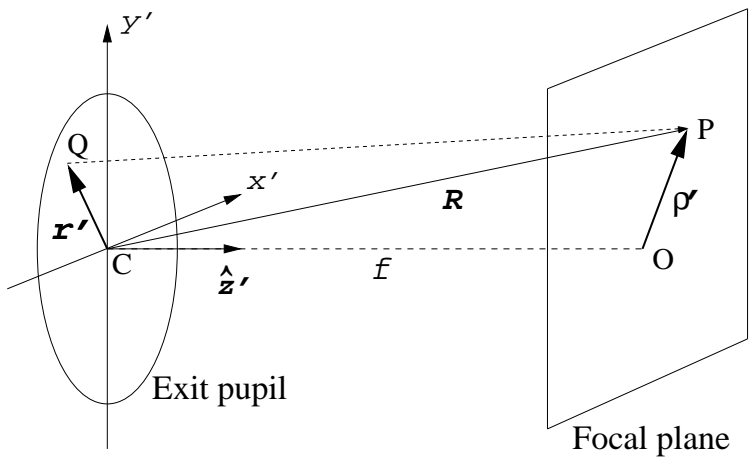


Fig. 3. Coordinate frame at exit pupil ( $x', y', z'$ ) and position,  $\rho'$ , of point  $P$

at focal plane. The field amplitude at point  $r'$  on the system's exit pupil is

$$E_{ex}(\mathbf{r}').$$

When considering the optical system in receiving mode, the PSF refers to the instantaneous field distribution in the focal plane of an optical imaging system produced by a far-field point source. For simplicity we assume that the fields are emerging from the exit pupil of the optical system with a system focal length  $f$ , and converging towards the image plane. Let's suppose that the exit pupil is on an infinite plane located at  $z = 0$ , and with the normal unit vector in direction of the z-axis,  $\hat{\mathbf{n}} = \hat{\mathbf{z}}'$  (see Fig. 3)<sup>1</sup>. Then, following Ref. 5,6, the scalar field at a point  $P$  at position  $\rho'$  in the paraxial focal plane (see Fig. 3) is given by

$$E_f(\rho') \propto \int_{AP'} E_{ex}(\mathbf{r}') e^{-j\frac{k}{f}\rho' \cdot \mathbf{r}'} dS' \quad (24)$$

where  $E_{ex}$  is the field amplitude at a point  $Q$  at position  $\mathbf{r}'$  on the system's exit pupil and  $f$  is also equal to the radius of curvature of the reference sphere centered at point  $O$  in the focal plane. In the case of a point source in the far field of the system  $E_{ex}$  is uniform over the pupil.

In Eq. (24) the substitution of the exit pupil for the antenna aperture plane, and the consequent use of  $\mathbf{r}'$  in both cases, is justified by using the *equivalent parabola* (e.g., in a dual-reflector system) and by the fact that when the point source object is at infinity, then the diameter (assuming a circular aperture) of the exit pupil can be substituted with the diameter of the entrance pupil, or main dish in a dual-reflector

---

<sup>1</sup>The focal plane and the observation point in the far-field defined by  $\hat{\mathbf{R}}$  in the previous sections (where the optical system was considered in transmission mode) lay on opposite directions with respect to the  $x'y'$  plane. This will be taken into account in Sect. 3.C

system (see Ref. 6, p. 184), and the system focal length would be in this case the focal length of the equivalent parabola.<sup>7</sup> In other words, the spherical (i.e., aberration-free) wavefront leaving the equivalent parabola and converging to the focus is identified here with the Gaussian reference sphere centred on the exit pupil. Then, we can state that *the (unaberrated) incoherent PSF is simply the square modulus of  $E_f(\rho')$ , i.e.,*

$$\text{PSF} = I(\rho') = |E_f(\rho')|^2.$$

Eq. (24) is strictly valid in the absence of phase errors that may modify the perfectly spherical convergent wave that was assumed earlier in the special case of an aberration-free wave-front. In the more general case of a distorted wave-front Eq. (24) should be re-written as:

$$E_f(\rho') \propto \int_{AP'} E_{ex}(\mathbf{r}') e^{-j\frac{k}{f}\rho' \cdot \mathbf{r}'} e^{j\Phi(\mathbf{r}')} dS' \quad (25)$$

where  $\Phi(\mathbf{r}')$  is the phase error term. The Strehl ratio,  $S$ , of the imaging system is then given by the ratio of the *central* (i.e.,  $\rho' = 0$ ) irradiance of its aberrated and unaberrated PSFs. From Eq. (25)  $S$  can be written in the form<sup>5,8</sup>:

$$S_o = \frac{I(0)}{I(0)|_{\Phi=0}} = \frac{\left| \int_{AP'} E_{ex}(\mathbf{r}') e^{j\Phi(\mathbf{r}')} dS' \right|^2}{\left| \int_{AP'} E_{ex}(\mathbf{r}') dS' \right|^2} \quad (26)$$

where  $S_o \equiv S(\rho' = 0)$ . The Strehl ratio can also be used as a measure of the on-axis PSF away from its central irradiance peak, and thus we can write:

$$S(\rho') = \frac{I(\rho')}{I(0)|_{\Phi=0}} =$$

$$= \frac{\left| \int_{AP'} E_{ex}(\mathbf{r}') e^{-j\frac{k}{f}\rho' \cdot \mathbf{r}'} e^{j\Phi(\mathbf{r}')} dS' \right|^2}{\left| \int_{AP'} E_{ex}(\mathbf{r}') dS' \right|^2}. \quad (27)$$

### 3.B. Strehl ratio off-axis

In equations (24) to (27) the position in the paraxial focal plane of the central irradiance peak of the PSF was taken as the origin of a Cartesian system of axes and also as the center of the (unaberrated) Gaussian reference sphere.<sup>8</sup> The observation of an object point off-axis, which is equivalent to having the feed lateraly displaced in a microwave antenna, introduces both a change in the position of the PSF peak (or direction of peak gain in an antenna) and wave-front aberration. The quasi-spherical (i.e., aberrated) wave will be thus converging to a point displaced with respect to point  $O$  in Fig. 3. If  $\rho'_{pk}$  represents the position of the off-axis PSF peak in the focal plane, then Eq. (27) can be re-written as:

$$\begin{aligned} S(\rho') &= \frac{I(\rho')}{I(\rho'_{pk})|_{\Phi_{ab}=0}} = \\ &= \frac{\left| \int_{AP'} E_{ex}(\mathbf{r}') e^{-j\frac{k}{f}\rho' \cdot \mathbf{r}'} e^{j\Phi(\mathbf{r}')} dS' \right|^2}{\left| \int_{AP'} E_{ex}(\mathbf{r}') e^{-j\frac{k}{f}\rho'_{pk} \cdot \mathbf{r}'} e^{j\Phi_1(\mathbf{r}')} dS' \right|^2} \end{aligned} \quad (28)$$

where  $\Phi_{ab}$  and  $\Phi_1(\mathbf{r}')$  have been defined in Eq. (12) and Sect. 2.B. Thus,  $I(\rho'_{pk})|_{\Phi_{ab}=0}$  represents the peak irradiance of the *unaberrated*, off-axis PSF.

In Sect. 2.B we saw that by tilting the aperture plane so that it becomes perpendicular to the direction of the peak gain, it is possible to write the aperture efficiency

in terms of  $\Phi_{ab}$  only. Likewise, in the definition of the PSF it is possible to align the  $z$ -axis along the direction from the center of the exit pupil to the off-axis Gaussian image point, which can also be taken as the origin of a new Cartesian system of axes. The Gaussian image point is also the center of curvature of the (tilted) wave front, and for this point all path lengths from the spherical wave front would be equal, in the absence of higher-order phase distortions. Then, Eq. (28) takes the same form as Eq. (27), i.e.

$$\begin{aligned} S(\boldsymbol{\rho}) &= \frac{I(\boldsymbol{\rho})}{I(0)|_{\Phi_{ab}=0}} = \\ &= \frac{\left| \int_{AP} E_{ex}(\mathbf{r}) e^{-j\frac{k}{f}\boldsymbol{\rho} \cdot \mathbf{r}} e^{j\Phi_{ab}(\mathbf{r})} dS \right|^2}{\left| \int_{AP} E_{ex}(\mathbf{r}) dS \right|^2} \end{aligned} \quad (29)$$

where the peak of the PSF is now at point  $\boldsymbol{\rho} = 0$  in the new system of axes, centered on the Gaussian image point in the focal plane, and  $\mathbf{r}$  now lies on a tilted plane,  $AP$ , perpendicular to the direction of the off-axis PSF peak. Thus we have in the projected plane,

$$\begin{aligned} S_o &= \frac{I(0)}{I(0)|_{\Phi_{ab}=0}} = \\ &= \frac{\left| \int_{AP} E_{ex}(\mathbf{r}) e^{j\Phi_{ab}(\mathbf{r})} dS \right|^2}{\left| \int_{AP} E_{ex}(\mathbf{r}) dS \right|^2}. \end{aligned} \quad (30)$$

### 3.C. Strehl ratio and aperture efficiency

In this section we use the previous results to derive a relationship between aperture efficiency and Strehl ratio. First, we use Eq. (13) to form the ratio of the aberrated

and unaberrated aperture efficiency (in the projected aperture plane), i.e.

$$\frac{\eta_A(\theta, \phi)}{\eta_{MP}} = \frac{\left| \int_{AP} \mathcal{E}_a(\mathbf{r}, \hat{\mathbf{R}}) dS \right|^2}{\left| \int_{AP} E_a(\mathbf{r}) dS \right|^2}, \quad (31)$$

with

$$\eta_{MP} = \frac{\left| \int_{AP} E_a(\mathbf{r}) dS \right|^2}{A_g \int_{\infty} E_a^2(\mathbf{r}) dS} \quad (32)$$

where  $\eta_A(\hat{\mathbf{R}}) \equiv \eta_A(\theta, \phi)$  is the aberrated aperture efficiency measured in the generic direction  $\hat{\mathbf{R}} = (\theta, \phi)$  (i.e., not coincident with the direction of the peak gain,  $\hat{\mathbf{R}}_{pk}$ ), for the general case in which the direction of peak-gain is not along the main optical axis of the system, as explained in Sect. 2.B.  $\eta_{MP} \equiv \eta_A(\hat{\mathbf{R}}_{pk})|_{\Phi_{ab}=0}$  is the unaberrated aperture efficiency measured in the direction of the (off-axis) peak gain, i.e.  $\eta_{MP}$  represents the peak aperture efficiency as measured in the projected aperture plane. Recalling that in the direction of the peak-gain  $\hat{\mathbf{R}}_{pk} \cdot \mathbf{r} = 0$  (see Sect. 2.C) the  $\hat{\mathbf{R}}$ -dependence can be dropped from  $\eta_{MP}$ . From eqs. (10) and (15) it also follows that,

$$\eta_{MP} = \eta_M \cos \theta_{pk} \simeq \eta_M \quad (33)$$

if  $\theta_{pk} \ll 1$ , where  $\eta_M$  is the maximum aperture efficiency as defined in Sect. 2.A.

From Eq. (32) and equations (17) and (18) we also see that  $\eta_M = \eta_{spill} \eta_{taper}$ .

Then, we note that equations (29) and (31) have the same form and, for small angles close to the optical axis it holds that

$$\boldsymbol{\alpha} \cdot \mathbf{r} = -\hat{\mathbf{R}} \cdot \mathbf{r}$$

where we have defined  $\alpha = \rho/f$  (see the discussion in Ref. 9). However, since  $E_{\text{ex}}$  represents the field produced by a point source in the far field of the system, in order to conclude that equations (29) and (31) are fully equivalent one must assume that the incident field on the optical system from a distant source has an apodization equivalent to that produced by the feed illumination on the antenna aperture (see Sect. 3.A). In this case we can write  $E_{\text{ex}}(\mathbf{r}) = E_a(\mathbf{r})$ , and thus

$$\eta_A(\hat{\mathbf{R}}) = \eta_M S(\boldsymbol{\rho}). \quad (34)$$

Then, by comparing equations (16) to (19) with Eq. (34) one can see that in general,

$$\eta_M S(\boldsymbol{\rho}) = \eta_{\text{spill}} \eta_{\text{taper}}(\hat{\mathbf{R}}) \eta_{\text{phase}}(\hat{\mathbf{R}}). \quad (35)$$

Usually, however, one is interested in the aperture efficiency at the nominal position of the peak gain (i.e., at the center of the far-field beam), or equivalently at the center of the PSF, then it also holds that

$$\begin{cases} \eta_o = \eta_M S_o \\ \eta_M = \eta_{\text{spill}} \eta_{\text{taper}} \end{cases} \quad (36)$$

and

$$S_o = \eta_{\text{phase}} \quad (37)$$

with  $\hat{\mathbf{R}}_{\text{pk}} \cdot \mathbf{r} = 0$  and  $\eta_o = \eta_A(\hat{\mathbf{R}} = \hat{\mathbf{R}}_{\text{pk}})$  is the aperture efficiency in the direction of the peak-gain, corresponding to Eq. (8) in the projected aperture plane, i.e.

$$\eta_o = \frac{\left| \int_{AP} E_a(\mathbf{r}) e^{j\Phi_{ab}(\mathbf{r})} dS \right|^2}{A_g \int_{\infty} E_a^2(\mathbf{r}) dS} \quad (38)$$

where we have not used the subscript “ $p$ ” (for “projected parameter”) in  $\eta_o$  because of the approximation in Eq. (33). Therefore, *Eq. (37) finally shows the equivalence between the Strehl ratio and phase efficiency.*

Clearly,  $\eta_M$  takes into account both taper and spillover effects, whereas  $S_o$  is a measure of the phase aberrations. Therefore, in the case of an *unaberrated* wave front, i.e.  $S_o = \eta_{\text{phase}} = 1$ , the aperture efficiency is  $\eta_o = \eta_M$  and depends only on the spatial distribution of the field over the antenna aperture. Furthermore, by explicitly writing the aberration function,  $\Phi_{ab}(\mathbf{r})$ , in terms of the primary aberrations (e.g., see Ref. 5) it would be possible to derive the individual contributions to the aperture efficiency by, e.g., coma, astigmatism and curvature of field, which are usually the most relevant aberrations in radiotelescopes. However, this is beyond the scopes of this work and will not be done here.

#### **4. Comparison of Strehl ratio and aperture efficiency**

In this section we want to compare the values of the Strehl ratio, obtained from a ray-tracing optical software, ZEMAX (Focus Software<sup>10</sup>), and the associated value of  $\eta_{\text{phase}}$ , obtained through the numerical integration of Eq. (19) and using the aperture field values computed by a Physical Optics program, GRASP9.3 (TICRA Engineering Consultants<sup>11</sup>). Several configurations have been analysed and are discussed below.

#### *4.A. Description of software packages*

The analysis has been conducted using the GRASP9.3 package, which is a commercial tool for calculating the electromagnetic radiation from systems consisting of multiple reflectors with several feeds and feed arrays. This package can use several high-frequency techniques for the analysis of large reflector antennas, such as Physical Optics (PO) supplemented with the Physical Theory of Diffraction (PTD), Geometrical Optics (GO) and Uniform Geometrical Theory of Diffraction (GTD), which require a moderate computational effort.

The PO technique is an accurate method that gives an approximation to the surface currents valid for perfectly conducting scatterers which are large in terms of wavelengths. The PO approximation assumes that the current in a specific point on a curved but perfectly conducting scatterer is the same as the current on an infinite planar surface, tangent to the scattering surface. For a curved surface, the PO current is a good approximation to the actual one if the dimensions of the scattering surface and its radius of curvature are sufficiently large measured in wavelengths. The well-known GO method uses ray-tracing techniques for describing wave propagation. Since GO gives discontinuities in the total electromagnetic field, GTD is often applied in addition to GO, since GTD methods may account for diffraction effects.

On the other hand, ZEMAX is a classical optical design tool based on ray-tracing methods, which combines three major categories of analysis in one package: lens

design, physical optics, and non-sequential illumination/stray light analysis.

#### *4.B. Calculation of the aperture efficiency with GRASP9.3*

As described in Sect. 4.A, GRASP9.3 allows several methods for the electromagnetic analysis of the reflecting surfaces. An interesting tool of GRASP9.3, based on the ray-tracing, for calculating the aperture field is the so-called “Surface Grid”.<sup>12</sup> This method returns the reflected magnetic field on the surface according to the formula:

$\mathbf{H}_r = \mathbf{H}_i - 2\hat{\mathbf{n}}(\hat{\mathbf{n}} \cdot \mathbf{H}_i)$ , where  $\mathbf{H}_i$  is the magnetic incident field and  $\hat{\mathbf{n}}$  is the normal to the surface. The magnetic reflected field on the surface,  $\mathbf{H}_r$ , is then projected, with a phase adjustment, on the aperture plane. As described in Sect. 2.B, when the feed is placed off-axis the aperture plane is tilted according to the direction of the peak-gain. For a dual reflector configuration, the scattering from the secondary and primary mirrors has been analyzed through the GTD technique and the “Surface Grid”, respectively.

This approach is particularly appropriate when the diameter-to-wavelength ratio of the primary reflector is very large and when the observation point is in the near-field (such as the aperture plane case). Under these conditions the PO method would be very time-consuming; in fact, it would require a huge number of points on the reflector where currents need to be evaluated. Using the method described here to analyze the primary reflector the diffracted field from the edge of the reflector is not considered. However, the numerical results obtained with this “hybrid” technique

have been compared with those obtained by applying the PO method to both the primary and secondary mirrors, resulting in a very good agreement between the two methods.

In order to calculate the aperture efficiency from Eq. (31) we use the the complex electric field in the aperture plane, i.e.  $\mathcal{E}_a(\mathbf{r}, \hat{\mathbf{R}})$ , produced by GRASP9.3, which is tabulated through its real and imaginary components. These can then be used to calculate the amplitude and the phase function of the field. The complex electric field is finally read by a proprietary code which evaluates Eq. (19) in order to determine the phase efficiency.

#### *4.C. Comparison of results*

The values of the Strehl ratio and phase efficiency obtained with ZEMAX and GRASP9.3, respectively, have been compared using three different optical systems. These systems have been selected to represent standard telescope designs, and the frequencies used in the simulations cover the mm- and submm-wavelength regimes. For the electromagnetic analysis with GRASP9.3, we have always used a linearly polarized Gaussian feed. Although more realistic feed models to describe circular horns could be adopted, for the sake of comparison with ZEMAX and to avoid introducing any systematic error due to different feed illumination, we report the results obtained with a Gaussian model only. The level of apodization in ZEMAX has then been chosen to be consistent with that produced by the Gaussian feed-horn.

#### 4.C.1. Single-dish antenna

First, we have carried out the comparison in the simplest possible case, i.e. an unblocked spherical reflector antenna. This choice eliminates or minimises potential discrepancies due to different handling in ZEMAX and GRASP9.3 of effects such as multiple reflections, aperture blocking and diffraction at secondary surfaces.

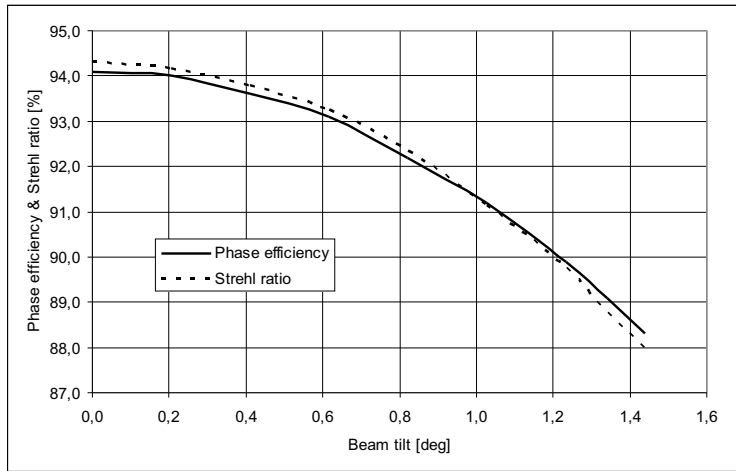


Fig. 4. Plot of the Strehl ratio and of the phase efficiency at a wavelength of  $500\mu\text{m}$  for the case of a spherical reflector  $105\text{ cm}$  in diameter with a  $f/\# = 2$ .

The surface chosen for this simulation is spherical because it ensures that spherical aberration will limit the overall FOV to small ( $\lesssim 1^\circ$ ) angles near the optical axis. This is required in order to avoid introducing further variables in the comparison between ZEMAX and GRASP9.3 due to the incidence angle of radiation over the aperture of the feed-horn in the focal plane, which may affect the coupling between the PSF and the electric fields on the horn aperture. The selected aperture was  $105\text{ cm}$  in diameter

with a  $f/\# = 2$  and the simulations have been carried out at a wavelength of 500  $\mu\text{m}$ . For the electromagnetic analysis with GRASP9.3, a linearly polarized Gaussian feed has been used with a taper level of  $-12 \text{ dB}$  at  $14^\circ$ .

The results are shown in Fig. 4: the comparison has been extended up to a maximum offset angle of  $\simeq 1.4^\circ$ , or about 44 beams at 500  $\mu\text{m}$ , and the maximum measured difference between the Strehl ratio calculated by ZEMAX and the phase efficiency calculated by GRASP9.3 is 0.38% at the maximum offset angle. We also note, however, a 0.25% discrepancy on boresight, which will be discussed in the next section.

#### 4.C.2. Dual-reflector antenna: Cassegrain configuration

We have then analysed the most common radio telescope design, consisting of a dual-reflector antenna. We first consider the classical Cassegrain configuration, which we have derived from the design of the “Balloon-borne Large Aperture Submillimeter Telescope” (BLAST) telescope.<sup>13</sup> Compared to the original design with a spherical primary mirror<sup>14</sup> and to the newer telescope design with a Ritchey-Chretien optical configuration, the system analysed here has a parabolic primary and a hyperbolic secondary. The diameters of primary and secondary mirrors are 181.61 and 42.76 cm, respectively, and the system focal ratio is 5. As in the single-reflector case, a linearly polarized Gaussian feed has been used, but with a taper level of  $-9 \text{ dB}$  at  $6^\circ$ .

The results are shown in Fig. 5: the comparison has been extended up to a maximum offset angle of  $\simeq 0.79^\circ$ , or about 42 beams at 500  $\mu\text{m}$ , thus quite equivalent to

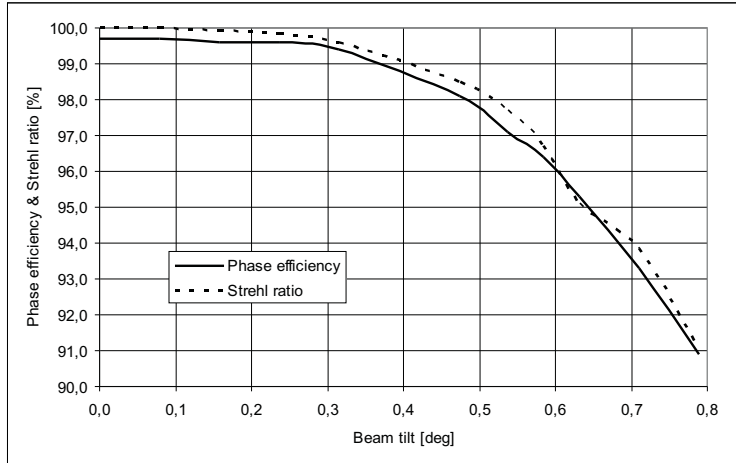


Fig. 5. Plot of the Strehl ratio and of the phase efficiency at a wavelength of  $500\mu\text{m}$  for the case of a classical Cassegrain telescope. The diameters of primary and secondary mirrors are 181.61 and 42.76 cm, respectively, and the system focal ratio is 5.

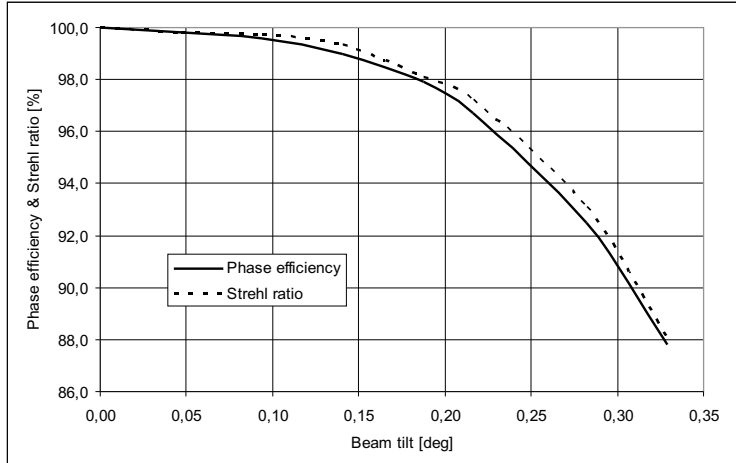


Fig. 6. Same as Fig. 5 for the scaled-up version of the BLAST telescope. The primary and secondary reflector diameters equal to 12.2m and 2.6m, respectively.

the previous simulation. The maximum measured difference between the Strehl ratio calculated by ZEMAX and the phase efficiency calculated by GRASP9.3 is about 0.59% at an offset angle of about  $0.5^\circ$ . We observe that the discrepancy between the two methods is also relevant ( $0.2 - 0.3\%$ ) for offset angles near boresight and it is possibly more systematic in this case than in the single-reflector design analysed in the previous section.

This on-axis difference is likely due to the relatively small secondary diameter to wavelength ratio,  $D_{\text{sec}}/\lambda$ , which may cause an on-axis decrease of the antenna gain due to diffraction effects from the edge of the secondary. To test this hypothesis, we have scaled-up the BLAST telescope, while keeping constant the wavelength, in order to obtain an optical design with a much larger  $D_{\text{sec}}/\lambda$  ratio, comparable to that used in the next section for the “Sardinia Radio Telescope”. We have thus obtained a telescope with the same focal ratio at the Cassegrain focus but with a primary and secondary reflector diameter equal to 12.2m and 2.6m, respectively.

The results are shown in Fig. 6: in this case the comparison has been extended up to a maximum offset angle of  $\simeq 0.33^\circ$ , or about 116 beams at  $500 \mu\text{m}$ . As expected, the discrepancy near the optical axis has decreased compared to both the single-dish and the original BLAST cases. The maximum difference is about 0.61%, thus still quite similar to that observed in the original BLAST design despite the much larger offset angle in beam units used in the scaled-up telescope. These results indicate that diffraction effects are calculated differently in GRASP9.3 and ZEMAX.

#### 4.C.3. Dual-reflector antenna: Gregorian configuration

The third system analysed during this comparison is another dual-reflector antenna, though in a Gregorian configuration. In this case we have changed the wavelength to a larger value of 3 mm and have also chosen a telescope with a much higher  $D/\lambda$  ratio. The baseline design is in this case the “Sardinia Radio Telescope” (SRT<sup>15</sup>); however, we have converted the original *shaped* design of the SRT to a more standard Gregorian configuration, keeping the same aperture (64 m) and system focal ratio (2.34) of the SRT. As in the previous two cases, a linearly polarized Gaussian feed has been used, with a taper level of  $-12$  dB at  $12^\circ$ .

The results are shown in Fig. 7: the comparison has been extended up to a maximum offset angle of  $\simeq 0.136^\circ$ , or about 42 beams at  $\lambda = 3$  mm, thus consistent with the simulations used for the single-dish and the BLAST configurations. The maximum measured difference between the Strehl ratio calculated by ZEMAX and the phase efficiency calculated by GRASP9.3 is about 1.9%, thus larger than in the optical systems discussed above. However, in the range of offset angles where the Strehl ratio (or equivalently the phase efficiency) is  $> 0.95$ , i.e. the range which is normally targeted by the optical design of diffraction-limited telescopes, the difference between Strehl ratio and phase efficiency is  $< 0.5\%$ , consistent with that observed in the BLAST telescope.

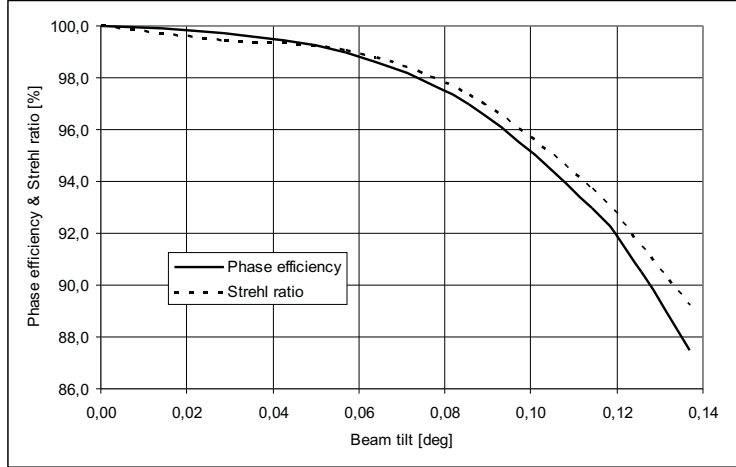


Fig. 7. Plot of the Strehl ratio and of the phase efficiency at a wavelength of 3 mm for the case of a classical Gregorian telescope, with a primary reflector diameter of 64 m and a system focal ratio of 2.34.

## 5. Conclusions

We have reviewed the main design parameters generally used in evaluating the performance of optical designs at both microwave and visible wavelengths. In particular, we have reviewed the classical concept of antenna gain and the main contributions to the aperture efficiency, with special attention to phase-error effects. We have then described the formalism with which to compare the aperture efficiency and its components with the Strehl ratio, which is the standard parameter used to evaluate the image quality of diffraction-limited telescopes at visible/IR wavelengths. We have shown that a simple relationship can be found between Strehl ratio and aperture efficiency: the Strehl ratio is equal to the phase efficiency when the apodization factor

is taken into account.

We have then compared these two parameters by running ray-tracing software, ZEMAX and full Physical Optics software, GRASP9.3, on three different telescope designs: a single spherical reflector, a Cassegrain telescope and finally a Gregorian telescope. These three configurations span a factor of  $\simeq 10$  in terms of  $D/\lambda$ . The simple spherical reflector allows the most direct comparison between Strehl ratio and phase efficiency, as it is only marginally affected by edge diffraction effects. In this case we find that these two parameters differ by less than 0.4% in our ZEMAX and GRASP9.3 simulations, up to an angle of about 44 beams off-axis. The other two configurations are more prone to diffraction effects caused by the secondary reflector, especially in the case of the smaller Cassegrain telescope.

The phase-efficiency is the most critical contribution to the aperture efficiency of the antenna, and the most difficult parameter to optimize during the telescope design. The equivalence between the Strehl ratio and the phase efficiency gives the designer/user of the telescope the opportunity to use the faster (and less expensive) commercial ray-tracing software to optimize the design using their built-in optimization routines.

### Acknowledgments

This work was partly sponsored by the Puerto Rico NASA Space Grant Consortium.

## References

1. S. Silver and H. James, eds., *Microwave Antenna Theory and Design* (Dover Publications, N.Y. (USA), 1949).
2. A.W. Rudge, K. Milne, A.D. Olver, and P. Knight, *The Handbook of Antenna Design*, Vol. 1 (P. Peregrinus Ltd., London (UK), 1982).
3. C.A. Balanis, *Antenna theory*, 2<sup>nd</sup> edition (J. Wiley & Sons, Inc., New York (USA), 1997).
4. J.W. Lamb, A.D. Olver, “Blockage due to subreflector supports in large radiotelescope antennas”, IEE Proc., Part H, **133**, N. 1, 43 (1986)
5. V. Mahajan, “Strehl ratio for primary aberrations: some analytical results for circular and annular pupils,” J. Opt. Soc. Am., **72**, 1258 (1982).
6. D. J. Schroeder, *Astronomical Optics* (Academic Press Inc., S. Diego (USA), 1987).
7. P. Hannan, “Microwave antennas derived from the cassegrain telescope,” IEEE Trans. Ant. Propagat., **9**, 140-153, 1961.
8. M. Born and E. Wolf, *Principles of Optics*, 4<sup>th</sup> edition (Pergamon Press Ltd., Oxford (UK), 1970).
9. R. Padman, “Optical fundamentals for array feeds,” in *Multi-feed Systems for Radio Telescopes*, D. T. Emerson, and J. M. Payne, eds. (ASP Conference Series, Vol. 75, San Francisco, 1995), pp. 3-26.

10. Focus Software, Inc., Tucson (USA), 2004.
11. TICRA Engineering Consultants, Copenhagen (Denmark), 2006.
12. TICRA Engineering Consultants, Reference Manual for GRASP9.3.
13. M.J. Devlin, and 26 coauthors, “The Balloon-borne Large Aperture Submillimeter Telescope (BLAST),” in *Millimeter and Submillimeter Detectors for Astronomy II*, J. Zmuidzinas, W.S. Holland, S. Withington, eds., Proc. SPIE **5498**, 42-54 (2004).
14. L. Olmi, “Optical designs for large detector arrays on spherical-primary orbital/sub-orbital telescopes,” Int. J. of Infrared and Millim. Waves, **22**, N. 6, 791 (2001).
15. G. Grueff, and 15 coauthors, “Sardinia Radio Telescope: the new Italian project,” in *Ground-based Telescopes*, J.M. Oschmann, Jr., eds., Proc. SPIE **5489**, 773-783 (2004).